



Nitrogen-doped carbon encapsulating molybdenum carbide and nickel nanostructures loaded with PVDF membrane for hexavalent chromium reduction

Yunjin Yao^{a,b,*}, Yi Hu^a, Maojing Yu^a, Chao Lian^a, Mengxue Gao^a, Jie Zhang^a, Guanwei Li^a, Shaobin Wang^{c,*}

^a Anhui Province Key Laboratory of Advanced Catalytic Materials and Reaction Engineering, School of Chemistry and Chemical Engineering, Hefei University of Technology, Tunxi Road 193, Hefei 230009, PR China

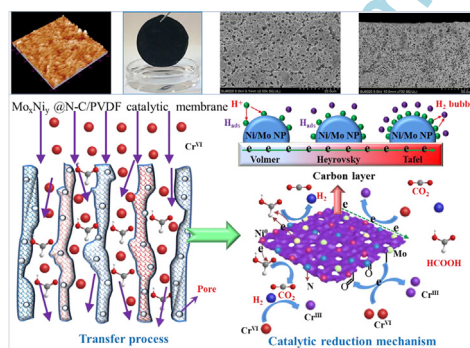
^b School of Chemistry and Material Science, University of Science and Technology of China, Hefei 230026, PR China

^c Department of Chemical Engineering, Curtin University, G.P.O. Box U1987, Perth, Western Australia 6845, Australia

HIGHLIGHTS

- Mo_xC and Ni^0 NPs embedding into N-doped carbon were prepared via pyrolysis.
- $\text{Mo}_x\text{Ni}_y@N\text{-C}$ was loaded on PVDF film to obtain the $\text{Mo}_x\text{Ni}_y@N\text{-C}/\text{PVDF}$ membranes.
- $\text{Mo}_x\text{Ni}_y@N\text{-C}/\text{PVDF}$ exhibited excellent catalytic activity for Cr^{VI} reduction.
- Membrane's porous structure minimizes NPs agglomeration and enhances mass transfer.
- The catalytic activities were closely related to the various operating parameters.

GRAPHICAL ABSTRACT



ARTICLE INFO

Keywords:

PVDF membrane
Hexavalent chromium
Molybdenum carbide
Reduction reaction

ABSTRACT

Molybdenum carbide and Ni^0 nanoparticles (NPs) embedding into N-doped carbon materials ($\text{Mo}_x\text{Ni}_y@N\text{-C}$) were prepared by one-step thermolysis of Ni, Mo, N, C precursors, and then loaded on poly(vinylidene fluoride) (PVDF) film to obtain the catalytic membranes ($\text{Mo}_x\text{Ni}_y@N\text{-C}/\text{PVDF}$). The membranes effectively catalyzed the reduction of toxic Cr^{VI} to benign Cr^{III} by employing formic acid (FA) as the reducing agent. The effects of parameters, such as initial concentrations of Cr^{VI} (5–25 mg/L) and FA (0.117–0.702 M), solution pHs (2.12–5.43) and temperatures (15–55 °C), as well as HCOONa concentrations (0–0.20 M) on Cr^{VI} reduction were analyzed in view of scalable industrial applications. Owing to the synergistic effects amongst Ni^0 , Mo_xC , doped nitrogen, and oxygen groups as catalytic active sites, and carbon shell protection of metal NPs from leaching out, $\text{Mo}_x\text{Ni}_y@N\text{-C}/\text{PVDF}$ catalysts exhibited excellent catalytic activity and recyclable capability for Cr^{VI} reduction. The membrane's unique porous structure and large chemically active surface area not only minimize the NPs agglomeration, but also allow the facile transport of catalytic reactants to the active surface without suffering from high

* Corresponding authors at: Anhui Province Key Laboratory of Advanced Catalytic Materials and Reaction Engineering, School of Chemistry and Chemical Engineering, Hefei University of Technology, Tunxi Road 193, Hefei 230009, PR China.

E-mail addresses: yaoyunjin@gmail.com (Y. Yao), shaobin.wang@curtin.edu.au (S. Wang).

<https://doi.org/10.1016/j.cej.2018.03.089>

Received 13 January 2018; Received in revised form 15 March 2018; Accepted 16 March 2018

Available online 17 March 2018

1385-8947/ © 2018 Elsevier B.V. All rights reserved.

mass-transfer resistance. This study demonstrates $\text{Mo}_x\text{Ni}_y\text{@N-C/PVDF}$ catalytic membranes with the morphological and structural features provide a green, economic, and fast method for the treatment of Cr^{VI} containing waters.

1. Introduction

Discharge of chromium into the environment is of growing worldwide concern for their high detrimental and toxic effects on human health and the environment [1,2]. In general, Cr^{VI} and Cr^{III} are the dominant species in the natural aquatic environment. Cr^{VI} is generally soluble, mobile in groundwater and surface water, whereas Cr^{III} usually forms insoluble $\text{Cr}(\text{OH})_3$ precipitates [3]. Cr^{VI} is a known carcinogen often found in water supplies both from human activities (e.g., electroplating, leather tanning, metal finishing, and chromium mining) and from the oxidation of Cr^{III} by natural processes, and has been listed as a prior pollutant by the U.S. Environmental Protection Agency [4]. Cr^{III} displays obviously lower toxicity compared to Cr^{VI} . Therefore, reduction of Cr^{VI} to Cr^{III} is a crucial motivation for Cr^{VI} decontamination.

Nowadays, different methods including chemical (adsorption and reduction), physical (electrical enrichment and washing), and biological processes, have been implemented to eliminate Cr^{VI} contamination [5]. Chemical reduction has great potential for the removal of Cr^{VI} and thus is attracting more and more attention, due to its considerable advantages in fastness, high efficiency, and eco-friendliness [6,7]. For reduction reaction, a catalyst with low overpotential and good reusability is vital. Recently, noble metals (e.g., Pt, Pd, Au, and Ag) have been received significant attention for Cr^{VI} reduction [8–10]. For example, Veerakumar et al. [4] reported that Pd@GAC exhibited an extraordinary activity for catalytic reduction of Cr^{VI} in the presence of formic acid (FA) as the reducing agent. The most benefit is that aqueous FA is an emerging reductant, thanks to its low cost, environmental friendliness and no secondary pollution [11]. Pd-based catalysts are the most effective materials, but their high cost and low abundance impeded the large-scale commercialization. Thus, it is critical to find novel and environmentally benign catalytic materials that use abundant elements and can be made by facile methods [12].

Because of the unique d-band electronic structures, molybdenum carbides (Mo_xC) have aroused ever-growing interest as high-performance catalysts. As such, it would be desirable to identify some innovative approaches for practical utilization by enhancing electron conduction through phase control, nanostructure and heterostructural engineering, intercalation, and doping. For example, Qiu et al. [13] found $\text{MoS}_2\text{@hybrid acid-doped polyaniline}$ immobilized on porous polyacrylonitrile nanofibers can efficiently remove toxic Cr^{VI} from aqueous environments. Similarly, Jiang et al. [14] found that Mo-driven composites could efficiently remove Cr^{VI} from aqueous solutions. Recently, Ni NPs-incorporated carbon composites have been proposed for FA-induced reduction of highly toxic aqueous Cr^{VI} [15]. Based on the theoretical calculations and experimental results, the synergistic effect of the metallic Ni and molybdenum compounds can enrich the electron density on the carbon surface, promoting hydrogen adsorption and evolution [16]. Some composites combining metallic Ni and molybdenum compounds, including Ni/NiMo₄N₅ [17], $\text{Mo}_x\text{C-Ni@N-doped carbon vesicle}$ [16], and porous carbon-supported Ni/Mo₂C [18], have exhibited both good activity and acid stability. Many researchers found that introduction of another element into the lattice of a given material can effectively modify the electronic and chemical properties [19]. In view of the above considerations, one of the most promising technologies is chemically coupling Ni with Mo_xC to improve the catalytic activity. To our knowledge, $\text{Mo}_x\text{C-Ni@N-doped carbon}$ has not been studied for Cr^{VI} removal.

Despite good performance of inexpensive nanomaterials, time-consuming and complicated separation procedures from the reaction system greatly limited their application. In order to solve these

problems, immobilizing nanocatalysts on porous membranes (e.g., renewable cellulose membrane, polycarbonate membrane, and porous ceramic membrane) offer a new way to achieve the separation and reuse [20,21]. In particular, poly(vinylidene fluoride) (PVDF) membrane has attracted much attention in wastewater purification, due to excellent mechanical strength and chemical stability [20,21]. For instance, we prepared iron NPs embedded carbon in PVDF membranes as a multifunctional catalytic system to effectively oxidize organic compounds [22]. Motivated by the studies, a material combining the redox reactivity of $\text{Mo}_x\text{C-Ni@N-doped carbon}$ with porous PVDF membranes is expected to show high Cr^{VI} removal capacity and efficiency.

In this study, we prepared molybdenum carbide and Ni⁰ NPs embedding into N-doped carbon materials ($\text{Mo}_x\text{Ni}_y\text{@N-C}$) through one-step thermal treatment, and then loaded on PVDF film to obtain the catalytic membranes ($\text{Mo}_x\text{Ni}_y\text{@N-C/PVDF}$). Then we used them as cost-effective and efficient catalysts for Cr^{VI} reduction using FA as a hydrogen donor. Varieties of physicochemical characterization techniques were performed to investigate the morphology, structure, surface compositions, and textural properties of the $\text{Mo}_x\text{Ni}_y\text{@N-C/PVDF}$ catalysts. The influences of several critical factors, such as initial concentrations of Cr^{VI} and FA, pHs, temperatures and HCOONa concentrations on Cr^{VI} reduction efficiency as well as the catalytic stability of the catalysts were systematically investigated. Moreover, a possible mechanism for the Cr^{VI} reduction was proposed.

2. Materials and methods

2.1. Chemicals and materials

All chemicals and materials were commercially available and used without further purification. Oxalic acid dihydrate ($\text{C}_2\text{H}_2\text{O}_4\cdot 2\text{H}_2\text{O}$), ammonium molybdate tetrahydrate ($(\text{NH}_4)_6\text{Mo}_7\text{O}_{24}\cdot 4\text{H}_2\text{O}$), melamine ($\text{C}_3\text{H}_6\text{N}_6$), nickel chloride hexahydrate ($\text{NiCl}_2\cdot 6\text{H}_2\text{O}$), polyvinylpyrrolidone (PVP), N, N-dimethylformamide (DMF), ethanol ($\text{C}_2\text{H}_6\text{O}$), potassium dichromate ($\text{K}_2\text{Cr}_2\text{O}_7$), formic acid (HCOOH, FA), hydrochloric acid (HCl), sodium hydroxide (NaOH) and sodium formate (HCOONa) were purchased from Sinopharm Chemical Reagent Co., Ltd. Poly(vinylidene fluoride) (PVDF) was purchased from Sigma-Aldrich Chemistry Co., Ltd.

2.2. Synthesis of $\text{Mo}_x\text{Ni}_y\text{@N-C}$ NPs catalysts

$\text{Mo}_x\text{Ni}_y\text{@N-C}$ NPs were synthesized through a simple pyrolysis route according to the published procedures [16]. Briefly, oxalic acid dihydrate (2.52 g, 0.02 mol) and ammonium molybdate tetrahydrate (0.27 g, 0.218 mmol) were firstly dissolved in 40 mL of deionized water. Secondly, melamine (1.26 g, 0.01 mol) was added to the above mixed suspension and refluxed at 70 °C for 6 h under stirring condition. Afterward, $\text{NiCl}_2\cdot 6\text{H}_2\text{O}$ (0.4 g, 1.68 mmol) was dissolved into the mixture solution, stirring for 12 h at room temperature. In addition, the solution was dried at 70 °C under vacuum, and then ground to obtain a fine powder. Subsequently, it was further put in an alumina crucible, heated to 900 °C in nitrogen atmosphere with a heating rate of 10 °C min⁻¹, and kept for 2 h. Unless noted otherwise, the products were denoted as $\text{Mo}_x\text{Ni}_y\text{@N-C}$ (where x and y represented the amounts (g) of Mo source ($(\text{NH}_4)_6\text{Mo}_7\text{O}_{24}\cdot 4\text{H}_2\text{O}$) and Ni source ($\text{NiCl}_2\cdot 6\text{H}_2\text{O}$), respectively).

2.3. Preparation of $\text{Mo}_x\text{Ni}_y@N\text{-C}/\text{PVDF}$ membranes

$\text{Mo}_x\text{Ni}_y@N\text{-C}$ blended PVDF catalytic membranes were fabricated by the phase inversion technique [22]. Briefly, 0.05 g of the synthesized $\text{Mo}_x\text{Ni}_y@N\text{-C}$, 0.25 g of PVP and 0.5 g of PVDF powder were totally dissolved in DMF (5 mL) solution with vigorous stirring at 60 °C for over 10 h to completely dissolve the polymer. Afterwards, the obtained solution was transferred into a drying oven for 12 h to remove air bubbles. After degassing, the solution was carefully poured into a Petri dish (24 cm²) with a controlled casting rate, and then immersed in a coagulation bath (ethanol aqueous solution at 25 °C) to induce phase inversion. The generated membranes labeled as $\text{Mo}_x\text{Ni}_y@N\text{-C}/\text{PVDF}$ were rinsed to remove the residual solvent and kept in deionized water before further use. Meanwhile, MoO_3 , NiO, and NiMoO_3 blended PVDF membranes (denoted as MoO_3/PVDF , NiO/PVDF , and $\text{NiMoO}_3/\text{PVDF}$) were also synthesized in the same way. The synthetic procedure of $\text{Mo}_x\text{Ni}_y@N\text{-C}/\text{PVDF}$ membranes is illustrated in Fig. 1.

2.4. Characterization

The surface and cross section morphologies of the as-obtained composites were investigated using field emission scanning electron microscopy (FE-SEM, SU8020, Hitachi, Japan). The field emission transmission electron microscopy (FE-TEM) observations were made using a JEOL JEM-2100 instrument at 200 kV. Energy dispersive X-ray spectra (EDS) and the elemental mapping were obtained from the randomly selected areas of each sample to probe the components of the elements. Powder X-ray diffraction (XRD) analysis was carried out by a Philips X'Pert Pro MPD diffractometer (40 kV, 40 mA; Cu K α radiation) with a scanning speed of 6° min⁻¹ over the range 5–90°. X-ray photoelectron spectroscopy (XPS) measurements were conducted on an ESCALAB250Xi spectrometer (Thermo Scientific, UK) with a monochromatic Al K α radiation. During the XPS analysis, the standard peak of carbon was set at 284.8 eV for charge corrections. Atomic force microscopy (AFM) measurements were recorded to measure the roughness of the samples with a CSPM4000 Scanning Probe Microscope (Benyuan, Beijing).

2.5. Cr^{VI} reduction tests

The catalytic activity was evaluated in a 250 mL conical flask containing 100 mL of Cr^{VI} solution prepared by adding potassium dichromate to the deionized water, which was shaken constantly in a thermostatic shaker. The catalytic membrane was firstly added to the bottle, followed by FA as the electron donor with an aliquot stock solution to initiate the reaction. For each sampling event, a volume of suspension was drawn from the reactor with a plastic syringe. The samples were immediately filtered through a 0.22 μm polytetrafluoroethylene (PTFE) membrane for chemical analysis. Cr^{VI} concentrations in the samples were determined by the absorbance of $\text{K}_2\text{Cr}_2\text{O}_7$ at 350 nm using an UV–vis spectrophotometer with 1 cm path length cuvettes. For a comparison study, control experiments were carried out using the different catalytic membranes in the presence or absence of FA. The influences of initial Cr^{VI} concentrations, FA concentrations, solution pHs, temperatures, and HCOONa concentrations on the efficiency of the Cr^{VI} reduction were carried out. To study the influence of solution pH on removal, the desired initial pH (pH_i) of each sample was adjusted to a value with droplet addition of HCl or NaOH, and the final pH (pH_o) was monitored through a pH meter. The catalytic durability of catalytic membrane was performed at least five times for any given conditions.

3. Results and discussion

3.1. Catalyst characterizations

The structural properties and chemical compositions of the as-prepared $\text{Mo}_x\text{Ni}_y@N\text{-C}$ samples were characterized by a variety of different physicochemical techniques. Representatively, the microstructures of the $\text{Mo}_{0.27}\text{Ni}_{0.4}@N\text{-C}$ NPs were firstly examined by FE-TEM and FE-SEM measurements. FE-SEM images show that the composite is assembled from NPs, forming a porous nanostructure (Fig. 2a), which is favorable for mass transport and reaction. FE-TEM image (Fig. 2b) reveals that the $\text{Mo}_{0.27}\text{Ni}_{0.4}@N\text{-C}$ heterostructures consist of inner Ni NPs and decorated Mo_xC NPs, and that both are encapsulated in the carbon matrices. Ni NPs were surrounded by Mo_xC NPs, benefiting electron transfer between them. Due to the good crystallinity, the lattice fringes could also be observed in the HRTEM image (Fig. 2c), in which the 2.04 Å could be assigned to the (1 1 1) interplane space of metallic Ni

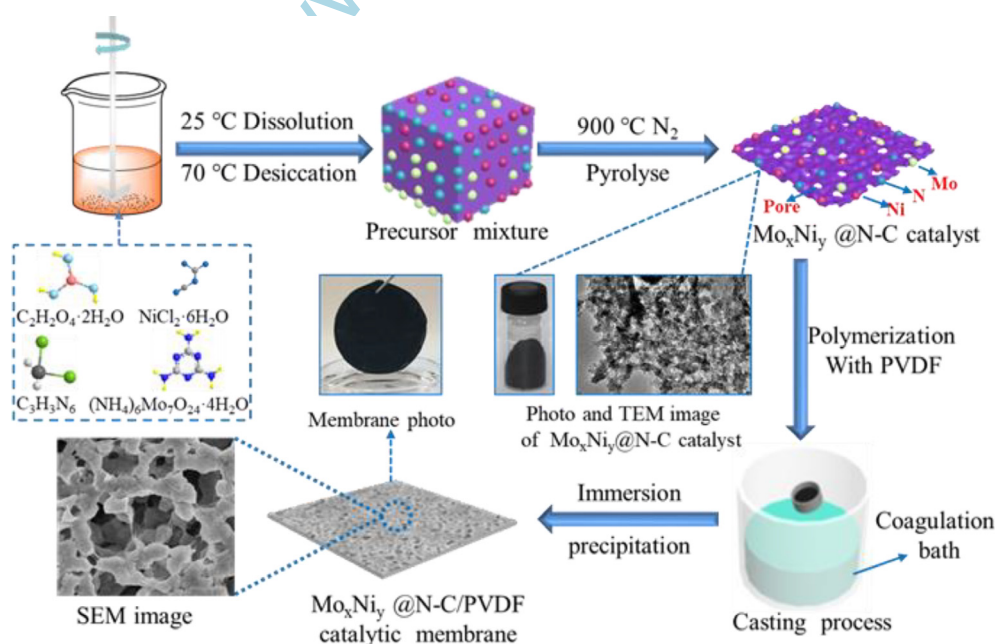


Fig. 1. Synthetic procedure of the $\text{Mo}_x\text{Ni}_y@N\text{-C}/\text{PVDF}$ membranes.

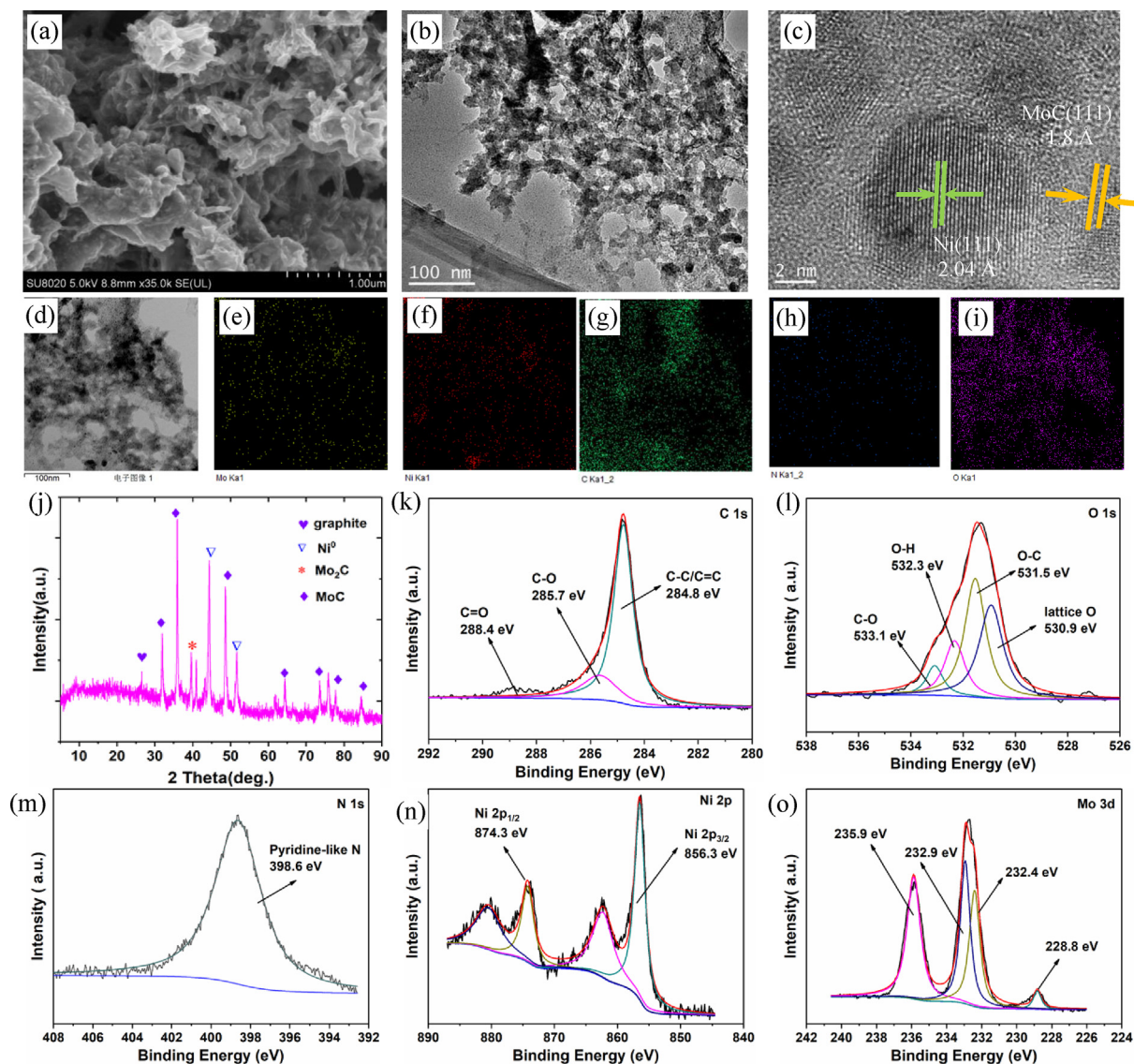


Fig. 2. Morphology and compositions of $\text{Mo}_{0.27}\text{Ni}_{0.4}@N\text{-C}$ NPs. (a) Representative FE-SEM image. (b) Representative FE-TEM image. (c) High-resolution TEM image. (d) FE-TEM image and its corresponding elements mapping: (e) Mo, (f) Ni, (g) C, (h) N, and (i) O elements. (j) XRD pattern. XPS spectra of (k) C 1s, (l) O 1s, (m) N 1s, (n) Ni 2p and (o) Mo 3d electrons.

and the 1.8 \AA belonged to the (1 1 1) plane of MoC. EDS analysis clearly shows the compositions of $\text{Mo}_{0.27}\text{Ni}_{0.4}@N\text{-C}$ comprising of Mo, Ni, C, N, and O elements (Fig. S1). The element mapping also demonstrates that molybdenum, nickel, carbon, nitrogen, oxygen species are distributed in the carbon matrix uniformly, indicating the nitrogen atom was successfully doped into the carbon lattice (Fig. 2d–i). All these results indicate that $\text{Mo}_{0.27}\text{Ni}_{0.4}@N\text{-C}$ is composed of typical Mo_xC and Ni, which are wrapped by carbon walls.

XRD pattern (Fig. 2j) confirms that sample $\text{Mo}_{0.27}\text{Ni}_{0.4}@N\text{-C}$ is composed of graphite, metallic Ni (JCPDS No. 04-0850), $\gamma\text{-MoC}$ (JCPDS No. 35-0787) and $\beta\text{-Mo}_2\text{C}$ (JCPDS No. 35-0787). The wide scan spectra of photoelectron peaks in Fig. S2 clearly show the presence of Mo 3d, Ni 2p, C 1s, N 1s, and O 1s. As shown in Fig. 2k, the high resolution XPS spectrum of the C 1s can be fitted into three peaks centered at 284.8, 285.7, and 288.4 eV, which can be attributed to C–C/C=C, C–O, and C=O species, respectively. Similarly, O 1s core level spectrum (Fig. 2l) can be divided into four peaks at $\sim 530.9 \text{ eV}$ (lattice O), $\sim 531.5 \text{ eV}$ (O–C), $\sim 532.3 \text{ eV}$ (O–H), and $\sim 533.1 \text{ eV}$ (C–O) [23]. The N 1s XPS spectrum (Fig. 2m) shows the peak is originated from the pyridinic N (398.6 eV). It is beneficial to the Cr^{VI} reduction caused by the lone pair electrons in the carbon matrix, which can withdraw electrons and

active hydrogen [24]. The Ni 2p spectrum is composed of two spin-orbit photoelectron peaks at 856.3 eV (Ni $2p_{3/2}$) and 874.3 eV (Ni $2p_{1/2}$) as well as their intense shakeup satellites, confirming the presence of Ni^{2+} in the composite (Fig. 2n) [25], which was possibly caused by the Ni–C bond on the surface of Ni NPs [16]. No obvious XPS signal of Ni^0 at 852.8 eV is observed, implying that Ni^0 NPs are encapsulated by the carbon layers. For the Mo 3d spectrum (Fig. 2o), two pairs of peaks (Mo $3d_{5/2}/3d_{3/2}$) at 232.9/235.9 and 228.8/232.4 eV can be ascribed to surface-oxidized MoO_x and Mo_2C , respectively [24]. The higher oxidation state of Mo may be caused by partial surface oxidation of the Mo_2C NPs, which was also observed in Mo_2C -type catalysts reported previously [24].

$\text{Mo}_{0.27}\text{Ni}_{0.4}@N\text{-C}$ NPs immobilized on a PVDF membrane are shown in Fig. 3. While the original PVDF membrane is porous, smooth, and white in color, the $\text{Mo}_{0.27}\text{Ni}_{0.4}@N\text{-C}/\text{PVDF}$ membrane becomes rough and uniformly black in color, indicating a uniform distribution of the $\text{Mo}_{0.27}\text{Ni}_{0.4}@N\text{-C}$ NPs on the PVDF scaffold (Fig. 3a). Fig. 3b, c present top layer and cross-sectional pore structure of the membranes casted by $\text{Mo}_{0.27}\text{Ni}_{0.4}@N\text{-C}$ NPs. It can be clearly observed that $\text{Mo}_{0.27}\text{Ni}_{0.4}@N\text{-C}$ was present on the membrane surface and inner pores, which enables facile transport and penetration of catalytic reactants to the active

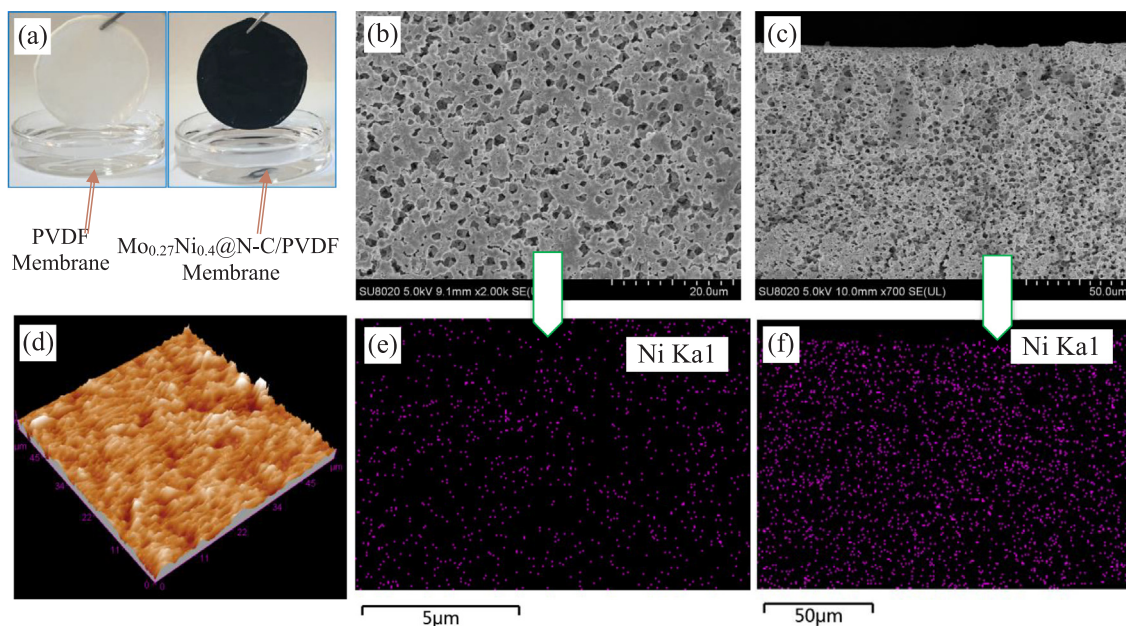


Fig. 3. Characterization of $\text{Mo}_{0.27}\text{Ni}_{0.4}@N\text{-C}/\text{PVDF}$ membrane: (a) Digital photographs; (b) FE-SEM top view; (c) FE-SEM cross-sectional view; (d) AFM 3D surface image; (e, f) EDS mapping from FE-SEM top and cross-sectional view.

surface without suffering from high mass-transfer resistance. During the membrane formation process, $\text{Mo}_{0.27}\text{Ni}_{0.4}@N\text{-C}$ NPs acted as pore forming centers, precipitated more slowly, and thus remained presence in the surface layer. Incorporation of NPs is recognized to improve pore formation and increases membrane hydrophilicity. EDS mapping analysis reveals that nickel is uniformly attached on the membrane surface (Fig. 3e, f). Such a unique structure may find applications in fast

catalytic reduction of contaminants. AFM indicates that $\text{Mo}_{0.27}\text{Ni}_{0.4}@N\text{-C}$ NPs have high surface roughness ($R_a = 77.2$ nm and $R_q = 102$ nm) (Fig. 3d). The high roughness could increase the efficient contact area, which led to the enhancement of the Cr^{VI} reduction. Totally, $\text{Mo}_{0.27}\text{Ni}_{0.4}@N\text{-C}$ NPs could improve the microstructure and influence the hydrophilicity of PVDF membranes.

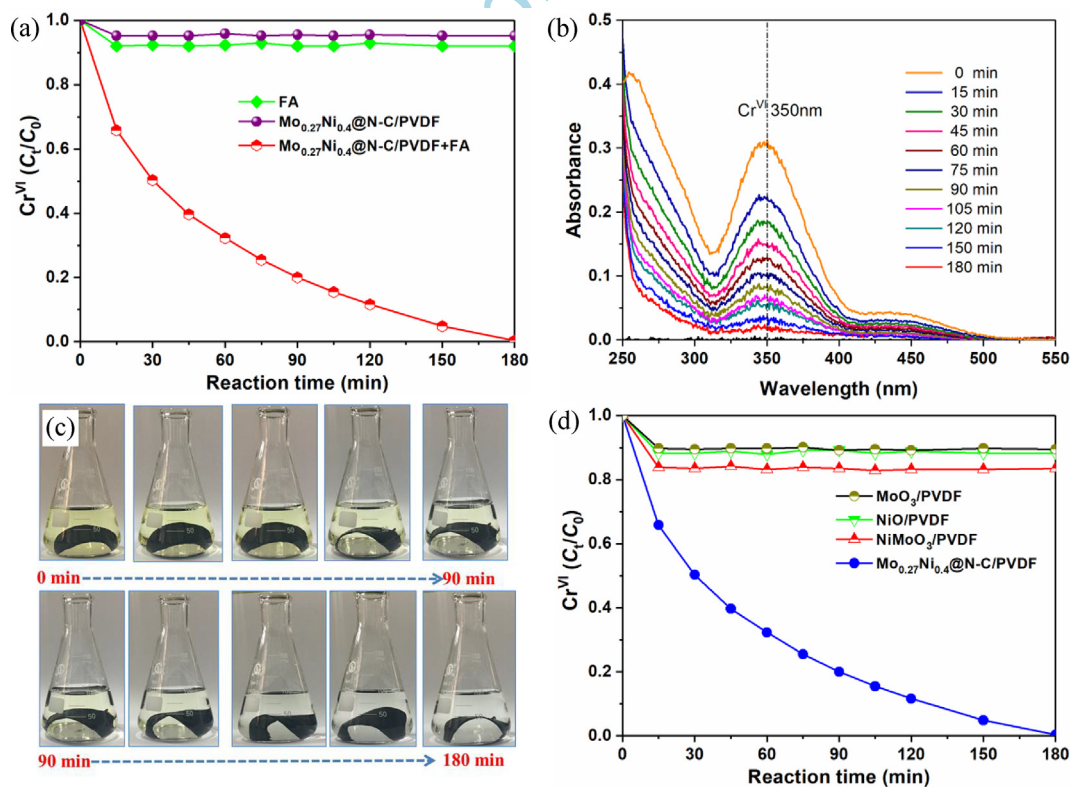


Fig. 4. (a) Comparison of the catalytic performance of samples under different conditions. (b) Decay of the UV-vis spectra of the Cr^{VI} solution in the presence of $\text{Mo}_{0.27}\text{Ni}_{0.4}@N\text{-C}$ NPs and FA. (c) Color changes of Cr^{VI} with the reaction times increasing. (d) Comparison of the catalytic activity of MoO_3/PVDF , NiO/PVDF , $\text{NiMoO}_3/\text{PVDF}$, and $\text{Mo}_{0.27}\text{Ni}_{0.4}@N\text{-C}/\text{PVDF}$ membranes. Experimental conditions: $[\text{Cr}^{\text{VI}}] = 10$ mg/L, $[\text{FA}] = 0.468$ M, $T = 25$ °C, without pH adjustment.

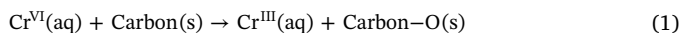
3.2. Catalytic evaluation

The catalytic activity of the membranes was studied by the Cr^{VI} reduction with FA as the reducing agent (Fig. 4a). We monitored the reaction progress by tracking the characteristic absorption of Cr^{VI} at 350 nm, originated from the ligand (oxygen) to metal (Cr^{VI}) charge transfer (LMCT) [11,26]. Less than 7.9% of Cr^{VI} reduction by FA alone indicated that the Cr^{VI} reduction by FA without metal catalysts was negligible. A control test using only Mo_{0.27}Ni_{0.4}@N-C membranes showed that less than 4.7% of Cr^{VI} could be adsorbed onto the surface in the absence of FA. Remarkably, nearly 100% of Cr^{VI} could be reduced within 180 min in the presence of Mo_{0.27}Ni_{0.4}@N-C/PVDF and FA. Thus, the catalytic property of the catalyst is crucial for efficient reduction of Cr^{VI}. Typically, the absorbance intensities of Cr^{VI} at 350 nm decreased successively after the introduction of Mo_{0.27}Ni_{0.4}@N-C/PVDF into the mixture solution containing Cr^{VI} and FA, and the color of the suspension solution changed typically from yellow to colorless with increasing reaction time, confirming the complete reduction of Cr^{VI} to Cr^{III} [4] (Fig. 4b,c). To confirm the presence of Cr^{III}, addition of sufficient NaOH in the colorless solution produced a color change from colorless to green (Fig. S3). It is known that FA is regarded as a hydrogen donor for Cr^{VI} reduction. Namely, FA is firstly decomposed to H₂ (HCOOH → H₂ + CO₂), which acts as the direct reducing agent for Cr^{VI} reduction [11]. The improved catalytic activity of Mo_{0.27}Ni_{0.4}@N-C/PVDF is largely attributed to its superior catalytic ability towards the decomposition of FA. In contrast, MoO₃/PVDF, NiO/PVDF, and NiMoO₃/PVDF presented poor catalytic activities under the same conditions (Fig. 4d).

The reusability of Mo_{0.27}Ni_{0.4}@N-C/PVDF membrane was performed under identical conditions. Very interestingly, no significant loss in reduction ability of Mo_{0.27}Ni_{0.4}@N-C/PVDF membrane was observed after five recycling tests (Fig. 5). The reduction efficiency of Mo_{0.27}Ni_{0.4}@N-C/PVDF membrane slightly decreased from nearly 100% to 82.3% in the five-cycle run, which was indicative of its high stability, even if compared with documented Pd-based catalysts [27]. From the XPS analyses (Fig. 6b), we found that trace amount of Cr^{VI} and Cr^{III} species existed on the surface of the used Mo_{0.27}Ni_{0.4}@N-C/PVDF catalysts. It is sure that the slight decrease in removal capacity can be ascribed to incomplete desorption. In view of high efficiency, cost-effectiveness, and good stability, the Mo_{0.27}Ni_{0.4}@N-C/PVDF membranes are promise materials for the fast removal of Cr^{VI} from aqueous solutions.

For the better illustration of the above-proposed reduction of Cr^{VI} to Cr^{III}, XPS analysis of the fresh and used Mo_{0.27}Ni_{0.4}@N-C/PVDF catalysts was carried out. Fig. S4 displays the spectra of Mo 3d, Ni 2p, C 1s, N 1s and O 1s in the fresh and used Mo_{0.27}Ni_{0.4}@N-C/PVDF samples. Fig. 6a shows a new peak occurring around the binding energy of 580 eV on the used sample. Further, the individual XPS scan for Cr 2p (Fig. 6b) shows the lowest binding energy band at 576.8 eV (Cr 2p_{3/2}-low) as well as the low Cr 2p_{1/2} component at 586.4 eV are correlated with the existence of Cr^{III} species. In addition, the higher Cr 2p_{3/2} band at 578.2 eV and the Cr 2p_{1/2} peak at 590.2 eV expose the presence of higher oxidation state Cr species, associated with Cr^{VI}. From the above, the accumulation of Cr^{III} on the surface of Mo_{0.27}Ni_{0.4}@N-C/PVDF after the reduction of Cr^{VI} can be concluded, which is very similar to a previous report [23]. That means the above evidence supports our proposed mechanism on the reduction of Cr^{VI} to Cr^{III} over the Mo_{0.27}Ni_{0.4}@N-C/PVDF composite. In addition, there are two peaks for the C 1s spectra (Fig. S4c) in both the fresh and used Mo_{0.27}Ni_{0.4}@N-C/PVDF samples: 284.8 eV assigned to C–C/C=C, and 289.3 eV assigned to C=O [28]. However, new peaks consisting of O=C (287.5 eV) and C–O (285.9 eV) appeared after the reduction reaction. The results suggested that the C=C bonds in Mo_{0.27}Ni_{0.4}@N-C were oxidized to C–O and C=O by Cr^{VI}, and that Cr^{III} ions were produced (Eq. (1)) [29,30]. XPS spectra of Mo 3d, Ni 2p, C 1s, N 1s and O 1s in Fig. S4 show almost no changes after the reaction. The above results indicate

that Mo_{0.27}Ni_{0.4}@N-C/PVDF is truly stable and robust for practical and perspective applications.



According to the above studies, the influences of the textural properties and compositions of the Mo_xNi_y@N-C/PVDF materials on the highly catalytic activity were comprehensively analyzed. The catalytic Cr^{VI} reduction curves of Mo_xNi_y@N-C/PVDF obtained at different mass ratios of Mo/Ni are shown in Fig. 7a. Fig. S5 shows the XRD patterns of these samples. The crystal Ni, Mo_xC contents, and graphitization degree were influenced by the introduction of Ni salts. Catalytic performance increased with the increased mass ratios of Mo/Ni up to 0.27:0.4 and decreased thereafter. It is quite interesting to note that the reduction process was fitted well with the pseudo-first-order reaction and the corresponding kinetic constants (*k*_{obs}) were given in Fig. 7b. In addition, the half-life *t*_{1/2}, defined as the related time at which half of the initial Cr^{VI} was degraded completely, can be obtained using Eq. (2):

$$t_{1/2} = \ln(2)/k_{\text{obs}} \quad (2)$$

Table 1 shows the parameter values estimated for the pseudo-first-order model applied to the experimental data. No noticeable adsorption of Cr^{VI} on any Mo_xNi_y@N-C/PVDF was observed (Fig. S6), indicating that the decrease in Cr^{VI} concentrations was due to the catalytic reduction of Cr^{VI} not to adsorption on the particles. Therefore, it is concluded the change of the mass ratios of Mo/Ni remarkably influences the catalytic activity, attributing to the distinct differences in the catalyst structures (such as metal content, nitrogen content, nitrogen type, and carbon structure). These results clearly suggest that the mass ratio of the precursors could play a crucial role in the Cr^{VI} reduction.

Furthermore, the roles of metallic Ni NPs and Mo_xC were also investigated (Fig. 7c, d). With only Ni modification, XRD pattern (Fig. S7) confirms that Mo₀Ni_{2.4}@N-C contains graphite and metallic Ni (JCPDS No. 04-0850). With only molybdenum modification, XRD pattern confirms that Mo_{2.7}Ni₀@N-C contains graphite, MoO₃ (JCPDS No. 21-0569), β-Mo₂C (JCPDS No. 35-0787), MoO₂ (JCPDS No. 78-1073) and Mo₂N_{0.76} (JCPDS No. 65-6236). The catalytic activity suggests that Mo_{0.27}Ni_{0.4}@N-C/PVDF is also much better than Mo₀Ni_{0.4}@N-C/PVDF and Mo_{0.27}Ni₀@N-C/PVDF, which can be inferred that the greatly high activity of the Mo_{0.27}Ni_{0.4}@N-C/PVDF materials mainly depended on the co-modification of molybdenum carbide and Ni. The mass ratio of Mo/Ni in Mo_xNi_y@N-C/PVDF was kept at 0.27:0.4 in all of the following experiments.

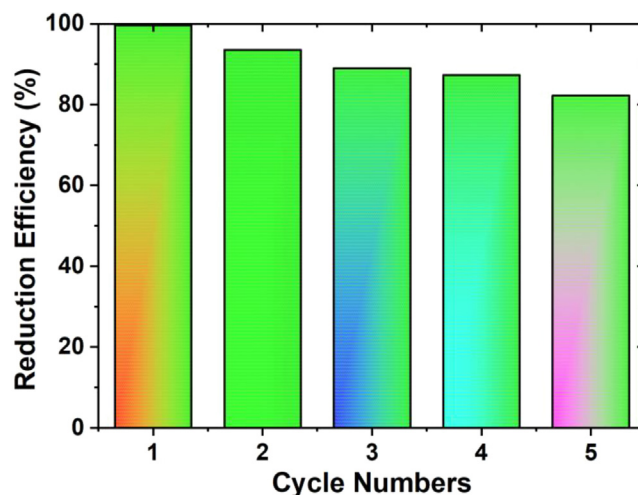


Fig. 5. Recycle experiments for Cr^{VI} solution using Mo_{0.27}Ni_{0.4}@N-C/PVDF and FA. Experimental conditions: [Cr^{VI}] = 10 mg/L, [FA] = 0.468 M, T = 25 °C, without pH adjustment.

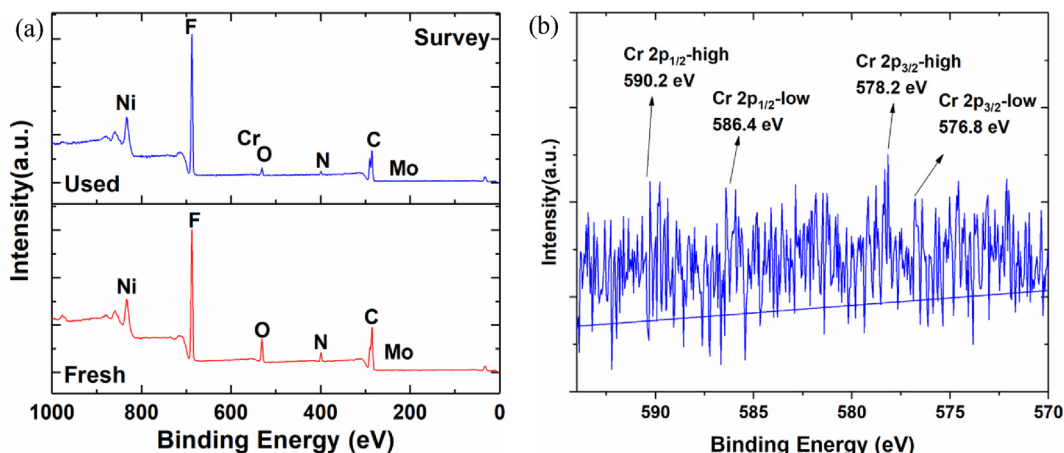


Fig. 6. (a) Full scan spectra for fresh and used $\text{Mo}_{0.27}\text{Ni}_{0.4}@N\text{-C}/\text{PVDF}$. (b) Cr 2p XPS spectrum for the used $\text{Mo}_{0.27}\text{Ni}_{0.4}@N\text{-C}/\text{PVDF}$.

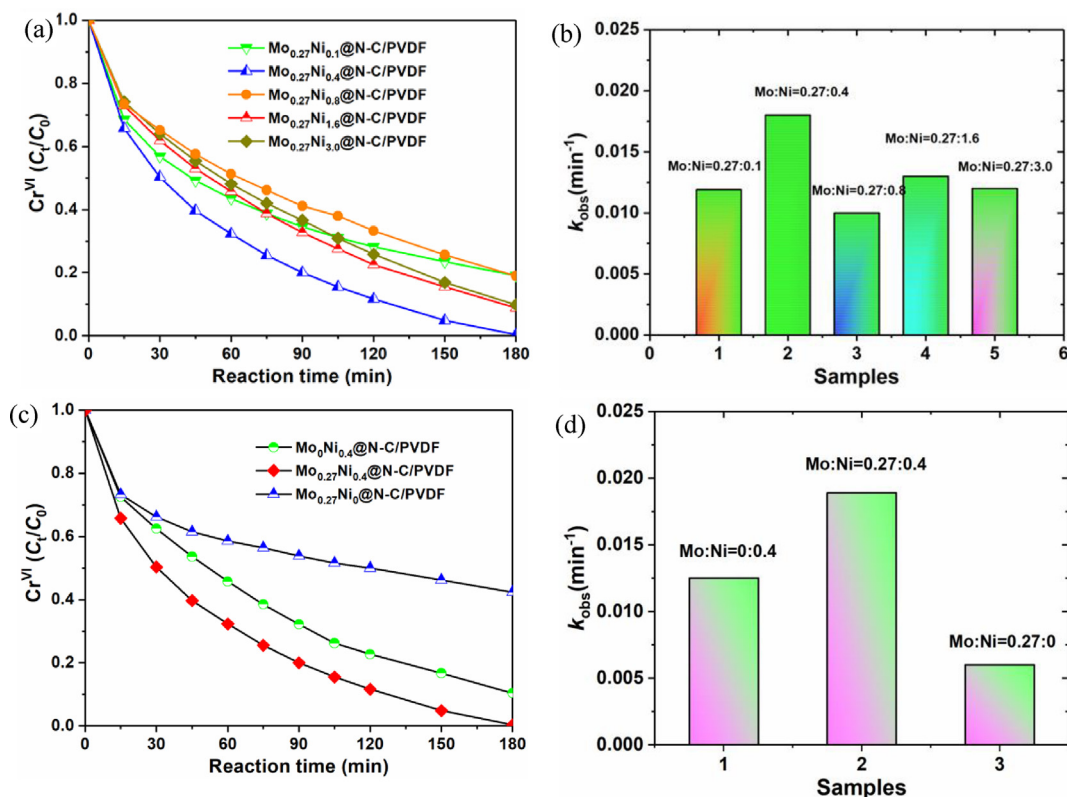


Fig. 7. (a, c) Comparison of the catalytic activity of $\text{Mo}_x\text{Ni}_y@N\text{-C}/\text{PVDF}$ prepared at different mass ratios of Mo/Ni. (b, d) The corresponding kinetic constants. Experimental conditions: $[\text{Cr}^{\text{VI}}] = 10 \text{ mg/L}$, $[\text{FA}] = 0.468 \text{ M}$, $T = 25^\circ\text{C}$, without pH adjustment.

Table 1

Kinetic rate constants for the Cr^{VI} reduction in the presence of FA and $\text{Mo}_x\text{Ni}_y@N\text{-C}/\text{PVDF}$ catalysts prepared at different mass ratios of Mo/Ni^a.

Catalysts	R ²	k_{obs} (min ⁻¹)	$t_{1/2}$ (min)
$\text{Mo}_{0.27}\text{Ni}_{0.1}@N\text{-C}/\text{PVDF}$	0.972	0.0119	58.2
$\text{Mo}_{0.27}\text{Ni}_{0.4}@N\text{-C}/\text{PVDF}$	0.996	0.018	38.5
$\text{Mo}_{0.27}\text{Ni}_{0.8}@N\text{-C}/\text{PVDF}$	0.982	0.01	69.3
$\text{Mo}_{0.27}\text{Ni}_{1.6}@N\text{-C}/\text{PVDF}$	0.995	0.013	53.3
$\text{Mo}_{0.27}\text{Ni}_{3.0}@N\text{-C}/\text{PVDF}$	0.994	0.012	57.8
$\text{Mo}_{0.27}\text{Ni}_0@N\text{-C}/\text{PVDF}$	0.923	0.006	115.5
$\text{Mo}_0\text{Ni}_{0.4}@N\text{-C}/\text{PVDF}$	0.996	0.0125	55.5

^a Experimental conditions: $[\text{Cr}^{\text{VI}}] = 10 \text{ mg/L}$, $[\text{FA}] = 0.468 \text{ M}$, $T = 25^\circ\text{C}$, without pH adjustment.

3.3. Effects of reaction parameters on Cr^{VI} reduction efficiency

The optimal sample of $\text{Mo}_{0.27}\text{Ni}_{0.4}@N\text{-C}/\text{PVDF}$ was selected to study the influences of several critical factors, such as initial FA concentrations, Cr^{VI} concentrations, reaction temperatures, initial pHs, and HCOONa concentrations on catalytic reduction of toxic Cr^{VI} to Cr^{III} . An increase in FA concentrations (0.117–0.702 M) had a positive effect on Cr^{VI} reduction efficiency, ascribing to the formation of more amount of reactive species during the reaction (Fig. 8a and Table S1). The reduction rate gradually increased with FA concentrations, but not linearly. Hence, an optimized FA concentration was taken at 0.468 M. Fig. 8b and Table S1 show that the Cr^{VI} reduction rate decreased quickly with increasing initial Cr^{VI} contents. Within 120 min, total elimination of Cr^{VI} for the concentrations of 5, 10, 15, 20, and 25 mg L^{-1} could reach about 99.4%, 88.4%, 57.6%, 53.6%, and 52.6%,

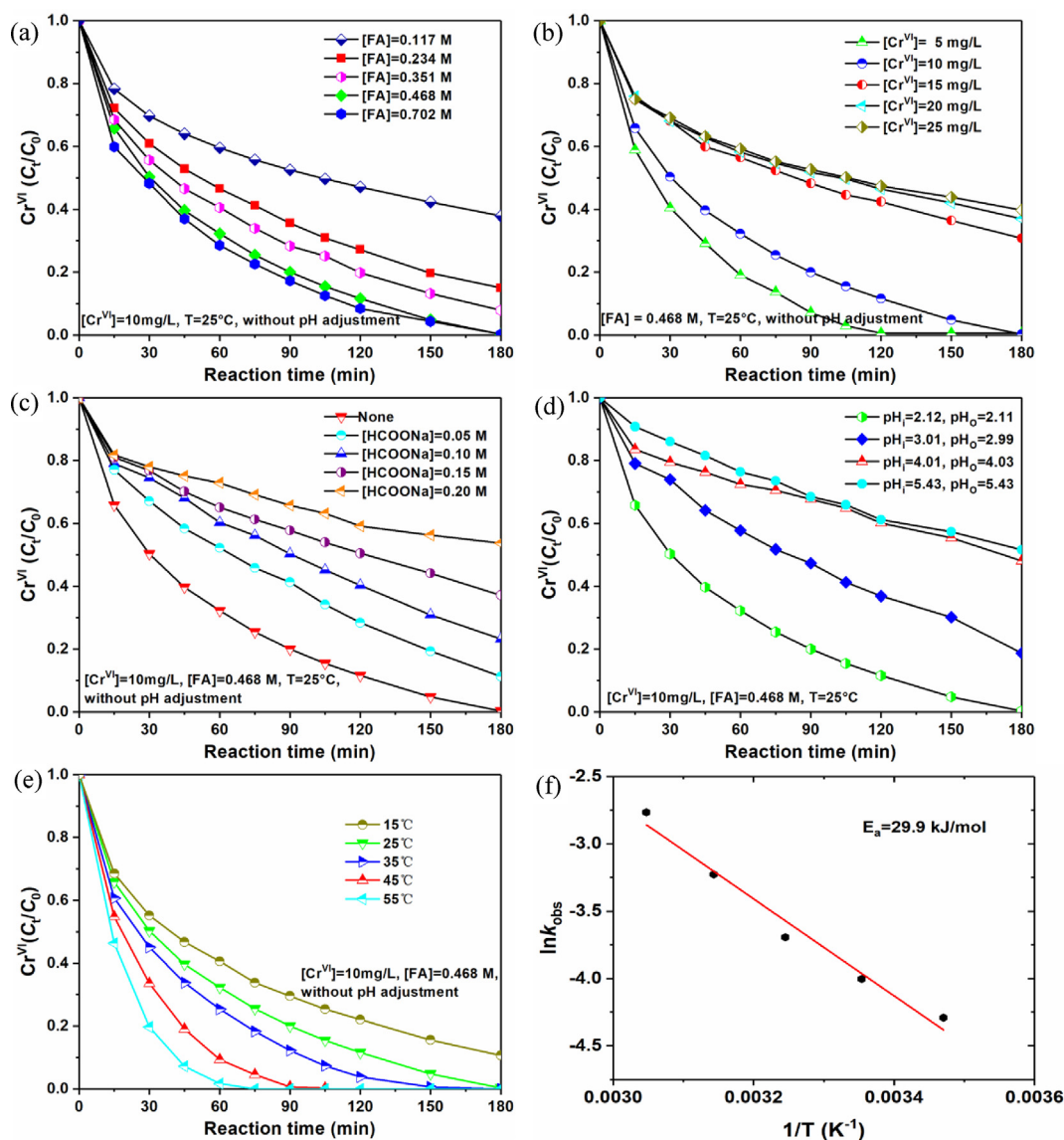


Fig. 8. Effect of (a) FA concentrations, (b) initial Cr^{VI} concentrations, (c) HCOONa concentrations, (d) initial pHs, and (e) reaction temperatures on the Cr^{VI} removal performance of the $\text{Mo}_{0.27}\text{Ni}_{0.4}@N\text{-C}/\text{PVDF}$ and FA system. (f) Arrhenius plot for the Cr^{VI} reduction using the $\text{Mo}_{0.27}\text{Ni}_{0.4}@N\text{-C}/\text{PVDF}$ and FA system. Experimental conditions: $[\text{Cr}^{\text{VI}}] = 10 \text{ mg/L}$, $[\text{FA}] = 0.468 \text{ M}$, $T = 25^\circ\text{C}$, without pH adjustment.

respectively. The intractability at the higher initial concentrations may be ascribed to the limited dosage of FA and the coverage of excess Cr ions on the active sites of the catalyst.

A recent report has pointed out HCOONa as a promoter can enhance the rate of formic acid decomposition [31]. The catalysts can liberate H_2 not only from FA but also from HCOONa through a catalytic hydrolysis ($\text{HCOONa} + \text{H}_2\text{O} \rightarrow \text{H}_2 + \text{NaHCO}_3$). For this reason, we performed a control experiment to check the HCOONa effect on reduction rate. As shown in Fig. 8c and Table S1, Cr^{VI} reduction was remarkably inhibited and reduction efficiency decreased from nearly 100% to 46.2% at HCOONa concentrations from 0 to 0.20 M, attributing to HCOONa competition with Cr^{VI} for the active sites of $\text{Mo}_{0.27}\text{Ni}_{0.4}@N\text{-C}/\text{PVDF}$, different with the reported literature [31]. Such an impact may be due to two aspects. Since the Cr^{VI} species were adsorbed by the surface sites of the $\text{Mo}_{0.27}\text{Ni}_{0.4}@N\text{-C}/\text{PVDF}$ composite primarily through ion exchange and electrostatic interaction, other anions would potentially be strong competitors [13].

Fig. 8d and Table S1 present the pH effect on the Cr^{VI} reduction efficiency over a range of pH values from 2.12 to 5.43. The pH of the dichromate solution was 4.94. After the addition of FA, the pH of the

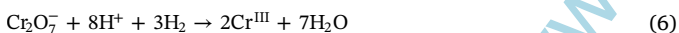
solution decreased to 2.12. In this case, FA maintains the pH of the reaction mixture and behaves as a reducing agent. At pHs of 2.12, 3.01, 4.01, and 5.43, Cr^{VI} reduction after 180 min reached 99.7%, 81.3%, 51.9%, and 48.4%, respectively. Cr^{VI} reduction decreased with the rise in the solution pH, consistent with several reports [32,33]. The pH dependence of Cr^{VI} reduction is mainly related to the ion (Cr^{VI}) chemistry in the solution. In aqueous solutions, Cr^{VI} dominantly exists as anionic species HCrO_4^- under acidic conditions. It is believed that the charge and charge distribution on the reaction, and dissociation of the hydrogen donor will also be affected by pH. Therefore, it could suggest that a higher pH gave the surface of $\text{Mo}_{0.27}\text{Ni}_{0.4}@N\text{-C}/\text{PVDF}$ less negative charges, which could greatly weaken the electrostatic interaction between the composite and HCrO_4^- anions, thus leading to the dramatically decreased reduction efficiency [13,34,35].

The effect of temperature was also investigated in the $\text{Mo}_{0.27}\text{Ni}_{0.4}@N\text{-C}/\text{PVDF}$ catalyzed reduction of Cr^{VI} by performing a series of experiments at various temperatures in the range of 15–55 °C (Fig. 8e and Table S1). It was found that the Cr^{VI} reduction rate increased quickly with the increase of reaction temperature, which demonstrates the endothermic nature of the reduction process. The k_{obs} values are used to

obtain Arrhenius plots (Fig. 8f) to calculate activation energy. The apparent activation energy (E_a) was estimated to be 29.9 kJ/mol, which is similar to the reported activation energy of Pd@SiO₂-NH₂ (25.9 kJ/mol) [36], Pd@ γ -Al₂O₃ (76.2 kJ/mol) [9] and Pd@TMV (27.3 kJ/mol) [10] catalysts for the same reaction. Considering the low cost and relatively high activity, Mo_{0.27}Ni_{0.4}@N-C/PVDF is a promising catalytic material for environmentally friendly reduction processes.

3.4. Reaction mechanism

On the basis of the above analyses, a mechanism on the Cr^{VI} reduction could be proposed and shown in Fig. 9. In the solution, Cr^{VI} exists in a soluble anionic form HCrO₄⁻. The positively charged surface of Mo_xNi_y@N-C/PVDF could effectively adsorb Cr^{VI} ions mainly through ion exchange and electrostatic attraction. In addition, FA was enriched on the surface of the Mo_xNi_y@N-C by simple electrostatic attraction. Cr^{VI} and FA in the solution were effectively transferred to the Mo_xNi_y@N-C NPs loaded on the porous PVDF membranes. After that, FA underwent a dehydrogenation decomposition pathway to produce CO₂ and H₂ [28,29]. Mo_xNi_y@N-C NPs are favorable to hydrogen evolution reaction due to their high efficiency [37,38]. First, a proton associates an electron and attaches on the catalyst surface (*) (Eq. (3)). After that, the adsorbed H tends to form H₂ via the Heyrovsky or Tafel route, and sequentially desorbs. The Heyrovsky route is referred to the reaction of the adsorbed H with a hydrated proton and receiving an electron from the catalyst surface (Eq. (4)), while the Tafel route is related to the direct combination of two adsorbed H atoms (Eq. (5)) [16]. In the presence of electron donating acids, the transformation of Cr^{VI} to less toxic Cr^{III} by the free hydrogen atom occurs and can be described by Eq. (6) [39]. In other words, the reduction step involves an electron-transfer process. For noble metal-based catalysts, Ni⁰ and Mo_xC have a strong enrichment capacity for hydrogen molecules, which can enhance the formation of atomic hydrogen [30].



The following aspects can explain the improved catalytic activity

and stability of Mo_xNi_y@N-C/PVDF membranes towards the Cr^{VI} reduction. First, metal-based nanocatalysts with a stable support provide enlarged active surface area, and more active atoms on the membrane surface, resulting in the enhancement of their catalytic activity. Second, the presence of porous structure of Mo_xNi_y@N-C/PVDF membranes enables facile transport and penetration of the reactant molecules to the active surface and to effectively capture Cr^{VI} from the external environment without suffering from high mass-transfer resistance. Third, the synergistic effects amongst Ni⁰, Mo_xC, doped nitrogen, and oxygen groups as catalytic active sites effectively improve the catalytic activity and recyclable capability for Cr^{VI} reduction performances. In addition, it is noteworthy that the Mo_xNi_y@N-C surface with a plenty of oxygen-containing groups such as carbonyl C=O, carboxy -COOH, and hydroxyl -OH, and a high proportion of the sp² carbon as the electron-transfer mediator can facilitate the electron transfer process from H₂ to Cr^{VI}, which may be responsible for an improved catalytic activity [11,30]. In particular, carbon shells could not only improve electrical conductivity, but also immobilize and protect the inner NPs from corrosion and agglomeration. Therefore, inherent nanosize effect of NPs and the porous structure of catalytic membrane could minimize the diffusion resistance for mass transfer and benefit the sufficient contact of reactants with the active sites, favoring the good catalytic performance [40].

4. Conclusions

In summary, we demonstrated that a novel PVDF membrane-supported Mo_xNi_y@N-C catalyst prepared by thermal treatment process could efficiently and robustly catalyze reduction of toxic Cr^{VI} to benign Cr^{III} using FA as a reducing agent. Hierarchical nanostructures were formed by uniformly anchoring Mo_xNi_y@N-C NPs on the PVDF membranes by the phase inversion technique. Owing to the synergistic effects amongst Ni⁰, Mo_xC, doped nitrogen, and oxygen groups as catalytic active sites, and carbon shell protection of metal NPs from leaching out, Mo_xNi_y@N-C/PVDF exhibited excellent catalytic activity and recyclable capability. The catalytic activities are closely related to the various operating parameters, such as initial concentrations of Cr^{VI} and FA, reaction temperatures, initial pHs, and HCOONa concentrations. Comparative analysis demonstrates the Mo_xNi_y@N-C/PVDF membranes have clear advantages over Mo_xNi_y@N-C NPs because of

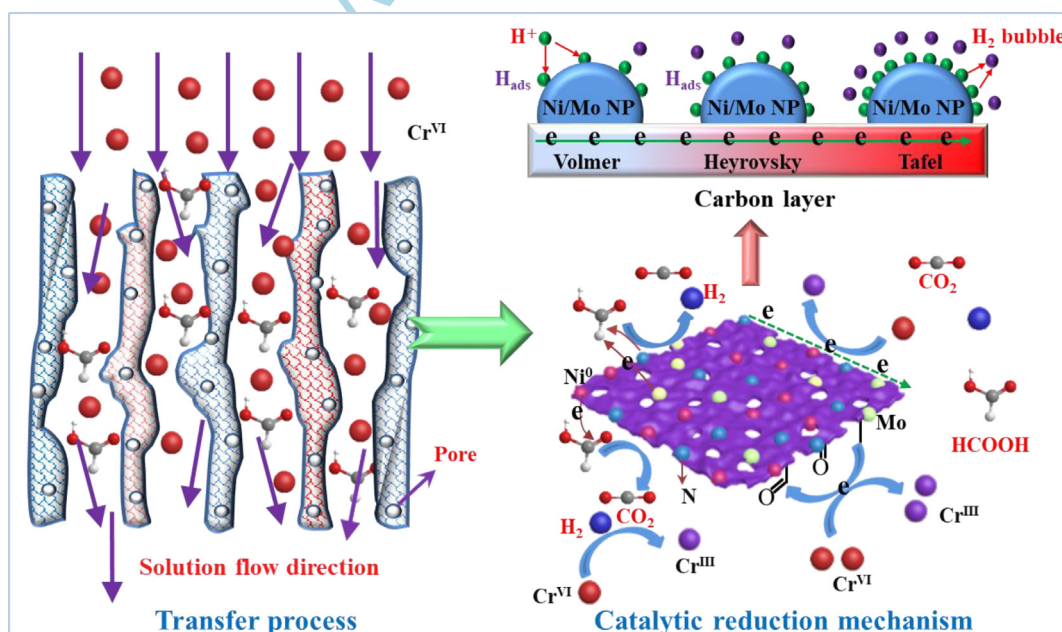


Fig. 9. Schematic illustration of the reaction mechanism for the Mo_xNi_y@N-C/PVDF and FA system.

higher $\text{Mo}_x\text{Ni}_y\text{@N-C/PVDF}$ catalytic activity, stable performance, and easily recycle. This work provides the cost-effective and efficient catalysts for water purification and might be expected to contribute to other important areas of environmental application. The development of this catalytic membrane for continuous-flow reaction and separation will be evaluated in the future.

Acknowledgements

The financial supports by the Anhui Provincial Natural Science Foundation (NO. 1708085MB41), the China Postdoctoral Science Foundation (NO. 2015M570547, 2016T90585), and Undergraduate Training Programs for Innovation and Entrepreneurship (NO. 2017CXCY049) are acknowledged. A partial support from the Australian Research Council for DP150103026 is also acknowledged.

Appendix A. Supplementary data

Supplementary data associated with this article can be found, in the online version, at <http://dx.doi.org/10.1016/j.cej.2018.03.089>.

References

- C. Pan, H. Liu, J.G. Catalano, A. Qian, Z. Wang, D.E. Giammar, Rates of Cr(VI) generation from $\text{Cr}_x\text{Fe}_{1-x}(\text{OH})_3$ solids upon reaction with manganese oxide, *Environ. Sci. Technol.* 51 (2017) 12416–12423.
- J.-C. Han, G.-J. Chen, L.-P. Qin, Y. Mu, Metal respiratory pathway-independent Cr isotope fractionation during Cr(VI) reduction by *Shewanella oneidensis* MR-1, *Environ. Sci. Technol. Lett.* 4 (2017) 500–504.
- C. Joe-Wong, G.E. Brown, K. Maher, Kinetics and products of chromium(VI) reduction by iron(II/III)-bearing clay minerals, *Environ. Sci. Technol.* 51 (2017) 9817–9825.
- P. Veerakumar, P. Thanasekaran, K.-C. Lin, S.-B. Liu, Biomass derived sheet-like carbon/palladium nanocomposite: an excellent opportunity for reduction of toxic hexavalent chromium, *ACS Sustainable Chem. Eng.* 5 (2017) 5302–5312.
- D. Wang, W. Guo, G. Zhang, L. Zhou, M. Wang, Y. Lu, D. Cai, Z. Wu, Remediation of Cr(VI)-contaminated acid soil using a nanocomposite, *ACS Sustainable Chem. Eng.* 5 (2017) 2246–2254.
- D. Wang, G. Zhang, L. Zhou, M. Wang, D. Cai, Z. Wu, Synthesis of a multifunctional graphene oxide-based magnetic nanocomposite for efficient removal of Cr(VI), *Langmuir* 33 (2017) 7007–7014.
- X.-L. He, Y.-P. Liu, K.-N. Gong, Z.-G. Han, X.-L. Zhai, Copper-organic cationic ring with an inserted arsenic-vanadium polyanionic cluster for efficient catalytic Cr^{VI} reduction using formic acid, *Inorg. Chem.* 54 (2015) 1215–1217.
- S.-H. Han, J. Bai, H.-M. Liu, J.-H. Zeng, J.-X. Jiang, Y. Chen, J.-M. Lee, One-pot fabrication of hollow and porous Pd-Cu alloy nanospheres and their remarkably improved catalytic performance for hexavalent chromium reduction, *ACS Appl. Mater. Interfaces* 8 (2016) 30948–30955.
- A. Dandapat, D. Jana, G. De, Pd nanoparticles supported mesoporous $\gamma\text{-Al}_2\text{O}_3$ film as a reusable catalyst for reduction of toxic Cr^{VI} to Cr^{III} in aqueous solution, *Appl. Catal. A: Gen.* 396 (2011) 34–39.
- C. Yang, J.H. Meldon, B. Lee, H. Yi, Investigation on the catalytic reduction kinetics of hexavalent chromium by viral-templated palladium nanocatalysts, *Catal. Today* 233 (2014) 108–116.
- L.-Y. Hu, L.-X. Chen, M.-T. Liu, A.-J. Wang, L.-J. Wu, J.-J. Feng, Theophylline-assisted, eco-friendly synthesis of PtAu nanospheres at reduced graphene oxide with enhanced catalytic activity towards Cr(VI) reduction, *J. Colloid Interface Sci.* 493 (2017) 94–102.
- L. Sun, C. Wang, Q. Sun, Y. Cheng, L. Wang, Self-assembly of hierarchical ni-mopolydopamine microflowers and their conversion to a Ni-Mo₂C/C composite for water splitting, *Chem. Eur. J.* 23 (2017) 4644–4650.
- J. Qiu, F. Liu, S. Cheng, L. Zong, C. Zhu, C. Ling, A. Li, Recyclable nanocomposite of flowerlike MoS₂@hybrid acid-doped PAN immobilized on porous PAN nanofibers for the efficient removal of Cr(VI), *ACS Sustainable Chem. Eng.* 6 (2017) 447–456.
- X. Jiang, H. Luo, Y. Yin, W. Zhou, Facile synthesis of MoS₂/reduced graphene oxide composites for efficient removal of Cr(VI) from aqueous solutions, *RSC Adv.* 7 (2017) 24149–24156.
- K. Bhowmik, A. Mukherjee, M.K. Mishra, G. De, Stable Ni nanoparticle-reduced graphene oxide composites for the reduction of highly toxic aqueous Cr(VI) at room temperature, *Langmuir* 30 (2014) 3209–3216.
- S. Wang, J. Wang, M. Zhu, X. Bao, B. Xiao, D. Su, H. Li, Y. Wang, Molybdenum-carbide-modified nitrogen-doped carbon vesicle encapsulating nickel nanoparticles: a highly efficient, low-cost catalyst for hydrogen evolution reaction, *J. Am. Chem. Soc.* 137 (2015) 15753–15759.
- T. Wang, X. Wang, Y. Liu, J. Zheng, X. Li, A highly efficient and stable biphasic nanocrystalline Ni-Mo-N catalyst for hydrogen evolution in both acidic and alkaline electrolytes, *Nano Energy* 22 (2016) 111–119.
- Z.-Y. Yu, Y. Duan, M.-R. Gao, C.-C. Lang, Y.-R. Zheng, S.-H. Yu, A one-dimensional porous carbon-supported Ni/Mo₂C dual catalyst for efficient water splitting, *Chem. Sci.* 8 (2017) 968–973.
- A.M. Gómez-Marín, E.A. Ticianelli, Effect of transition metals in the hydrogen evolution electrocatalytic activity of molybdenum carbide, *Appl. Catal. B: Environ.* 209 (2017) 600–610.
- C. Wang, Y. Wu, J. Lu, J. Zhao, J. Cui, X. Wu, Y. Yan, P. Huo, Bioinspired synthesis of photocatalytic nanocomposite membranes based on synergy of Au-TiO₂ and polydopamine for degradation of tetracycline under visible light, *ACS Appl. Mater. Interfaces* 9 (2017) 23687–23697.
- J. Wang, Z. Wu, T. Li, J. Ye, L. Shen, Z. She, F. Liu, Catalytic PVDF membrane for continuous reduction and separation of p-nitrophenol and methylene blue in emulsified oil solution, *Chem. Eng. J.* 334 (2018) 579–586.
- Y. Yao, C. Lian, Y. Hu, J. Zhang, M. Gao, Y. Zhang, S. Wang, Heteroatoms doped metal iron-polyvinylidene fluoride (PVDF) membrane for enhancing oxidation of organic contaminants, *J. Hazard. Mater.* 338 (2017) 265–275.
- Y. Yao, C. Lian, G. Wu, Y. Hu, F. Wei, M. Yu, S. Wang, Synthesis of “sea urchin”-like carbon nanotubes/porous carbon superstructures derived from waste biomass for treatment of various contaminants, *Appl. Catal. B: Environ.* 219 (2017) 563–571.
- C. Lu, D. Tranca, J. Zhang, F.N. Rodríguez Hernández, Y. Su, X. Zhuang, F. Zhang, G. Seifert, X. Feng, Molybdenum carbide-embedded nitrogen-doped porous carbon nanosheets as electrocatalysts for water splitting in alkaline media, *ACS Nano* 11 (2017) 3933–3942.
- J.-S. Wei, H. Ding, P. Zhang, Y.-F. Song, J. Chen, Y.-G. Wang, H.-M. Xiong, Carbon dots/NiCo₂O₄ nanocomposites with various morphologies for high performance supercapacitors, *Small* 12 (2016) 5927–5934.
- F.-Q. Shao, J.-J. Feng, X.-X. Lin, L.-Y. Jiang, A.-J. Wang, Simple fabrication of AuPd@Pd core-shell nanocrystals for effective catalytic reduction of hexavalent chromium, *Appl. Catal. B: Environ.* 208 (2017) 128–134.
- S. Li, L. Liu, Q. Zhao, C. He, W. Liu, N-doped graphene-supported PdCu nanoalloy as efficient catalyst for reducing Cr(VI) by formic acid, *PCPP* 20 (2018) 3457–3464.
- J. Yang, Y. Zhao, S. Ma, B. Zhu, J. Zhang, C. Zheng, Mercury removal by magnetic biochar derived from simultaneous activation and magnetization of sawdust, *Environ. Sci. Technol.* 50 (2016) 12040–12047.
- L. Zhou, G. Zhang, J. Tian, D. Wang, D. Cai, Z. Wu, Functionalized Fe₃O₄@C nanospheres with adjustable structure for efficient hexavalent chromium removal, *ACS Sustainable Chem. Eng.* 5 (2017) 11042–11050.
- J. Huang, Y. Cao, Q. Shao, X. Peng, Z. Guo, Magnetic nanocarbon adsorbents with enhanced hexavalent chromium removal: morphology dependence of fibrillar vs particulate structures, *Ind. Eng. Chem. Res.* 56 (2017) 10689–10701.
- L.-L. Wei, R. Gu, J.-M. Lee, Highly efficient reduction of hexavalent chromium on amino-functionalized palladium nanowires, *Appl. Catal. B: Environ.* 176–177 (2015) 325–330.
- L. Shi, T. Wang, H. Zhang, K. Chang, X. Meng, H. Liu, J. Ye, An amine-functionalized iron(III) metal-organic framework as efficient visible-light photocatalyst for Cr(VI) reduction, *Adv. Sci.* 2 (2015) 1500006–1500013.
- K. Zhu, C. Chen, H. Xu, Y. Gao, X. Tan, A. Alsaedi, T. Hayat, Cr(VI) reduction and immobilization by core-double-shell structured magnetic polydopamine@zeolitic imidazolate frameworks-8 microspheres, *ACS Sustainable Chem. Eng.* 5 (2017) 6795–6802.
- L. Zhuang, Q. Li, J. Chen, B. Ma, S. Chen, Carbothermal preparation of porous carbon-encapsulated iron composite for the removal of trace hexavalent chromium, *Chem. Eng. J.* 253 (2014) 24–33.
- X. Sun, Y. Yan, J. Li, W. Han, L. Wang, SBA-15-incorporated nanoscale zero-valent iron particles for chromium(VI) removal from groundwater: mechanism, effect of pH, humic acid and sustained reactivity, *J. Hazard. Mater.* 266 (2014) 26–33.
- M. Celebi, M. Yurderi, A. Bulut, M. Kaya, M. Zahmakiran, Palladium nanoparticles supported on amine-functionalized SiO₂ for the catalytic hexavalent chromium reduction, *Appl. Catal. B: Environ.* 180 (2016) 53–64.
- J. Wang, S. Mao, Z. Liu, Z. Wei, H. Wang, Y. Chen, Y. Wang, Dominating role of Ni⁰ on the interface of Ni/NiO for enhanced hydrogen evolution reaction, *ACS Appl. Mater. Interfaces* 9 (2017) 7139–7147.
- M. Miao, J. Pan, T. He, Y. Yan, B.Y. Xia, X. Wang, Molybdenum carbide-based electrocatalysts for hydrogen evolution reaction, *Chem. Eur. J.* 23 (2017) 10947–10961.
- A.K. Mishra, D. Pradhan, Morphology controlled solution-based synthesis of Cu₂O crystals for the facets-dependent catalytic reduction of highly toxic aqueous Cr(VI), *Cryst. Growth Des.* 16 (2016) 3688–3698.
- M. Liang, R. Su, W. Qi, Y. Zhang, R. Huang, Y. Yu, L. Wang, Z. He, Reduction of hexavalent chromium using recyclable Pt/Pd nanoparticles immobilized on procyranidin-grafted eggshell membrane, *Ind. Eng. Chem. Res.* 53 (2014) 13635–13643.